

# Shape of the chest wall in the prone and supine anesthetized dog

SUSAN S. MARGULIES AND JOSEPH R. RODARTE

*Division of Thoracic Diseases, Mayo Foundation, Rochester, Minnesota 55905; and Department of Medicine, Baylor College of Medicine, Houston, Texas 77030*

MARGULIES, SUSAN S., AND JOSEPH R. RODARTE. *Shape of the chest wall in the prone and supine anesthetized dog*. *J. Appl. Physiol.* 68(5): 1970-1978, 1990.—The shape of the passive chest wall of six anesthetized dogs was determined at total lung capacity (TLC) and functional residual capacity (FRC) in the prone and supine body positions by use of volumetric-computed tomographic images. The transverse cross-sectional areas of the rib cage, mediastinum, and diaphragm were calculated every 1.6 mm along the length of the thorax. The changes in the volume and the axial distribution of transverse area of the three chest wall components with lung volume and body position were evaluated. The decrease of the transverse area within the rib cage between TLC and FRC, as a fraction of the area at TLC, was uniform from the apex of the thorax to the base. The volume of the mediastinum increased slightly between TLC and FRC (14% of its TLC volume supine and 20% prone), squeezing the lung between it and the rib cage. In the transverse plane, the heart was positioned in the midthorax and moved little between TLC and FRC. The shape, position, and displacement of the diaphragm were described by contour plots. In both postures, the diaphragm was flatter at FRC than at TLC, because of larger displacements in the dorsal than in the ventral region of the diaphragm. Rotation from the prone to supine body position produced a lever motion of the diaphragm, displacing the dorsal portion of the diaphragm cephalad and the ventral portion caudad. In five of the six dogs, bilateral isovolume pneumothorax was induced in the supine body position while intrathoracic gas volume was held constant. The mediastinum fell toward the spine, but the rib cage was unaffected by pneumothorax. At TLC, the diaphragm was flatter after pneumothorax, presumably because the gradient in transdiaphragmatic pressure ( $P_{di}$ ) increased with pneumothorax. At FRC, the change of diaphragm shape with pneumothorax was smaller because the changes in the  $P_{di}$  were smaller compared with the mean  $P_{di}$ .

ventilation; rib cage; diaphragm

IT IS WIDELY BELIEVED that alterations in the shape of the chest wall distort the lung and affect regional ventilation (3, 5-7, 13, 14), but little information about the detailed shape of the chest wall is available. No information is available about the effect of the nonuniform distribution of pleural pressure in the intact animal on the shape of the thoracic cavity. We measured shapes of the rib cage, mediastinum, and diaphragm of anesthetized dogs by the use of the dynamic spatial reconstructor (DSR), a fast volumetric X-ray computed-tomographic scanner. The passive shapes of these components of the chest wall in supine and prone dogs at total lung capacity

(TLC) and at functional residual capacity (FRC) are reported. In the supine position, the shape of the thoracic cavity was also determined at these intrathoracic gas volumes after pleural pressure was made uniform by inducing isovolume pneumothorax. The changes in the shapes of the chest wall components with lung volume, body posture, and pneumothorax are described.

## METHODS

Six bred-for-research beagle dogs of either sex were anesthetized with 30 mg/kg pentobarbital, intubated with a no. 8 endotracheal tube, and placed supine in a volume displacement body plethysmograph. FRC was determined by Boyle's law when the animal attempted to inspire against an occluded airway. Inspiratory capacity (IC) and TLC were determined by measuring the volume change when airway pressure was raised to 30 cmH<sub>2</sub>O. The lung volume measurements were repeated with the animal lying prone.

On a separate occasion the dogs were anesthetized with intravenous barbiturate, supplemented as necessary during the course of the experiment, and intubated with an oral endotracheal tube. A latex esophageal balloon connected by a PE-200 catheter to a Validyne DP9 pressure gauge was placed in the middle third of the esophagus (Pes). Pressure at the oral end of the endotracheal tube was monitored by another DP9 pressure gauge ( $P_{ao}$ ). Signals from these transducers were recorded on a multichannel recorder, and transpulmonary pressure ( $P_{tp}$ ) was determined by on-line signal subtraction.

A small stainless steel screw was placed in the tip of an upper thoracic spinous process to serve as a fiducial marker. The animal was placed prone in a cloth sling in the DSR. The endotracheal tube was connected to a calibrated supersyringe and the IC required to increase the airway pressure to 30 cmH<sub>2</sub>O was determined to the nearest 100 ml. In all cases this volume was quite similar to the IC determined previously in the plethysmograph.

After two inflations with this IC, followed by spontaneous expirations back to FRC to establish a constant volume history and induce hyperventilation apnea, the dog's lungs were inflated a third time to TLC, and the thorax was scanned for 1 s. The lungs were then deflated with the calibrated syringe to the control FRC and scanned again. The FRC and inspiratory volumes are reported in Table 1. The inflation volumes were not

TABLE 1. *Body weights and lung volumes*

Dog No.	Body Weight, kg	IC,* ml	FRC, ml	
			Supine	Prone
1	12.25	700	407	407
2	16.0	650	403	399
3	13.0	700	438	431
4	12.0	700	378	346
5	12.5	700	468	440
6	14.5	900	521	516

Values are means of at least 3 measurements determined using volume displacement body plethysmograph. \* Syringe volume.

corrected for the opposing effects of humidity and gas compression.

The animal was rotated to the supine position, and the scan sequence was repeated. The same IC was used in the supine and prone positions. The airway pressures in the supine and prone positions at TLC were very similar.

The animal was again inflated twice to TLC and allowed to exhale passively to FRC. A lethal dose of barbiturate was then injected during the ensuing apnea. The animals all experienced immediate respiratory arrest and profound bradycardia, followed shortly by cardiac arrest, as judged by fluoroscopy. Shortly after the injection of the barbiturate the airway was connected to the supersyringe, which contained one IC, and the scan sequence was repeated postmortem. Throughout this scan sequence and the remainder of the experiment, the respiratory system and syringe formed a closed volume to ensure constant total volume. The respiratory system pressure-volume relationship during this maneuver with the closed system was not different than during life, indicating there was no significant respiratory gas uptake or alteration of the respiratory system mechanics because of postmortem muscle changes.

With the respiratory system volume at FRC, 2 mm OD polyethylene catheters, clamped closed proximal to their tips to prevent premature uncontrolled pneumothorax, were introduced bilaterally into the pleural space in the cephalic parasternal region through airtight O ring seals. The right and left pleural catheters (still clamped closed) were joined with a Y connector, which in turn was attached to the endotracheal tube and syringe via a Luer-Lok three-way stopcock. The absence of air leaks was confirmed by fluoroscopy and by constant esophageal and airway pressures during this procedure. The three-way stopcock was then opened and the clamps removed to allow air from the lungs to escape into the pleural space with no change in thoracic cavity volume. Equilibrium was established when airway opening pressure and pleural pressure were equal. The thoracic cavity was inflated slowly with the syringe, adding a volume equal to the control IC. During the supine isovolume pneumothorax  $P_{ao}$  was always within 0.5 cmH<sub>2</sub>O of  $P_{es}$ , indicating that equilibrium was achieved. When the lungs had completely collapsed, as judged by plateaus in  $P_{ao}$  and  $P_{es}$ , the thorax was scanned at TLC. Then a volume equal to IC was withdrawn slowly, and when equilibrium was reached the thorax was scanned at FRC.

One dog developed a system leak with the induction of pneumothorax, and pneumothorax data from this animal

are not presented. One animal was repositioned in the prone posture and scanned at TLC and FRC.

**Data analysis.** The TLC and FRC scanned images were reconstructed into 124 by 124 by 122 to 125 arrays of voxels or volume elements. The gray-scale value of each voxel represents the radiopacity of a 1.6-mm cubic element. The gray-scale data were transformed using an interactive thresholding routine to a binary image in which lung tissue was black and all other tissues were white. The lung cross-sectional area as a function of cephalocaudal position was computed by counting the black voxels in each 1.6-mm transverse slice and converting this number to square centimeters. Repeating the thresholding/counting process yielded values of cross-sectional area that differed by <3%. The cephalocaudal location of each cross-section from the lung apex, or  $z$  position in our coordinate system, was calculated from the slice number. An example of the distribution of cross-sectional area with  $z$  is shown in Fig. 1. Prone images were aligned with supine images using the spinal screws as fiducial markers. Total lung volume was calculated by multiplying the sum of the cross-sectional areas by the slice thickness. The calculated IC (the difference between the calculated TLC and FRC lung volumes) was within an average of 30 ml of the calibrated syringe volumes listed in Table 1. Previous studies have documented the accuracy of longitudinal and volumetric measurements in the DSR (4, 9).

The mediastinum-lung boundary was identified in the binary image using an interactive cursor routine, and the mediastinum cross-sectional area distribution was determined. Once counted, the mediastinum voxels were converted to black, making the entire thoracic cavity black, while the abdomen and rib cage remained white. The superior abdominal surface (the lung-apposed diaphragm) was identified in this binary image as the boundary between the black thorax and white abdomen, and

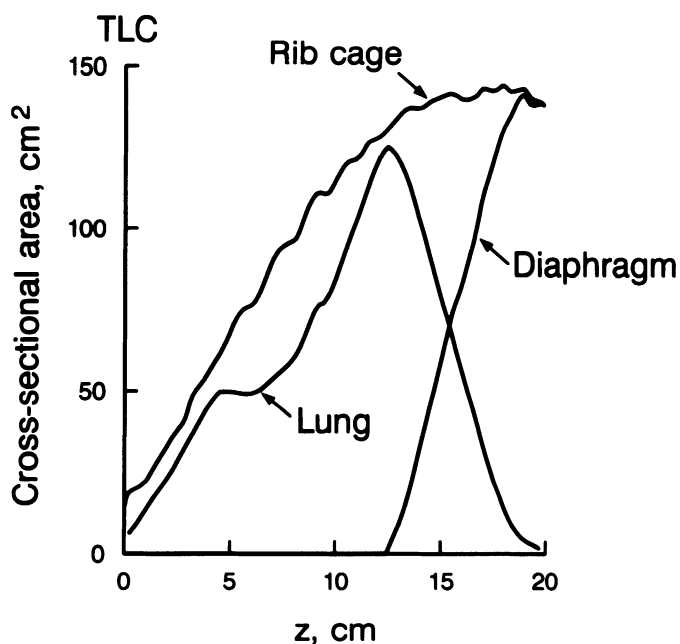


FIG. 1. Cross-sectional area of rib cage, lung, and diaphragm/abdomen at TLC in anesthetized dog as a function of  $z$ .

the lateral abdomen boundary was distinguished from the inner surface of the rib cage with the aid of the gray-level image. No attempt was made to identify position of the ring of insertion of the diaphragm. The white voxels in every slice within this diaphragm-abdomen boundary were counted. The cross-sectional area distribution of the diaphragm boundary is identified in Fig. 1. Together the lung, mediastinal, and abdominal contents fill the thorax to the inner surface of the rib cage, and the rib cage cross-sectional area shown in Fig. 1 is the sum of the cross-sectional areas of these three components.

## RESULTS

The results were quite consistent in all of the dogs, presumably because pure-bred dogs were used. The data from all successful experiments are included in the analysis. To illustrate the results, however, we present the data from *dog 4*, which was also studied in the prone position after induction of isovolume pneumothorax. Data from the other dogs are discussed only when differences arise.

The cephalocaudal distributions of rib cage, mediastinum, and diaphragm cross-sectional area at TLC and FRC in the anesthetized dog are presented for the supine and prone body positions in Fig. 2.

The cross-sectional area of the mediastinum is large in the midthorax where the heart is located and small in the cephalad and caudad portions of the thoracic cavity

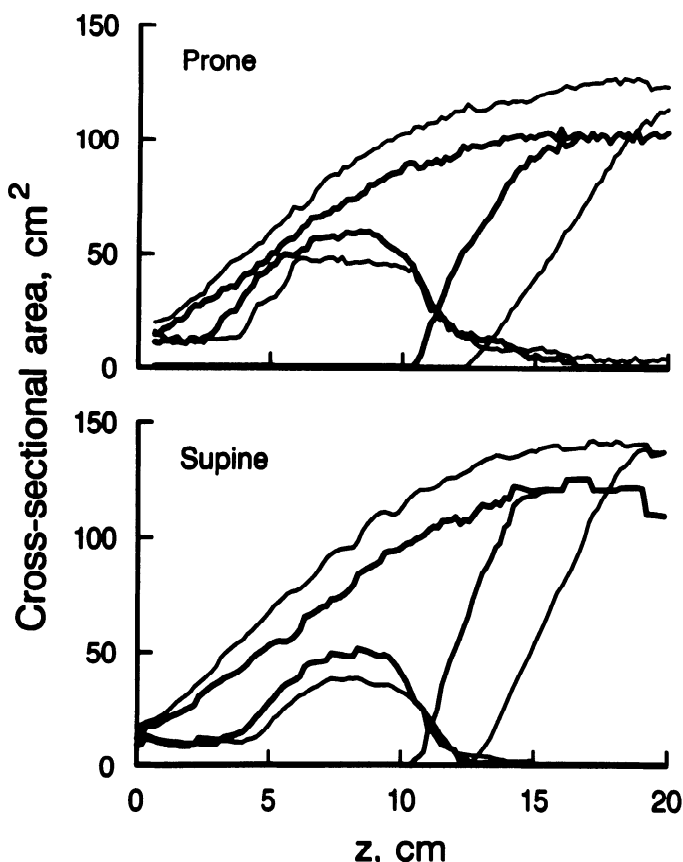


FIG. 2. Cephalocaudal cross-sectional area distribution of rib cage, mediastinum, and diaphragm at TLC (thin lines) and FRC (thick lines) in the prone and supine anesthetized dog. Prone and supine data were lined up by using fiducial markers.

TABLE 2. Mediastinum volume increase during passive deflation from TLC to FRC in the anesthetized dog

Dog No.	Supine		Prone	
	ml	%TLC volume	ml	%TLC volume
1	20	8	50	19
2	72	31	38	12
3	37	14	39	16
4	63	24	60	15
5	34	13	83	32
6	-14	-4	89	25
Means $\pm$ SD	35 $\pm$ 31	14 $\pm$ 12	60 $\pm$ 22	20 $\pm$ 7

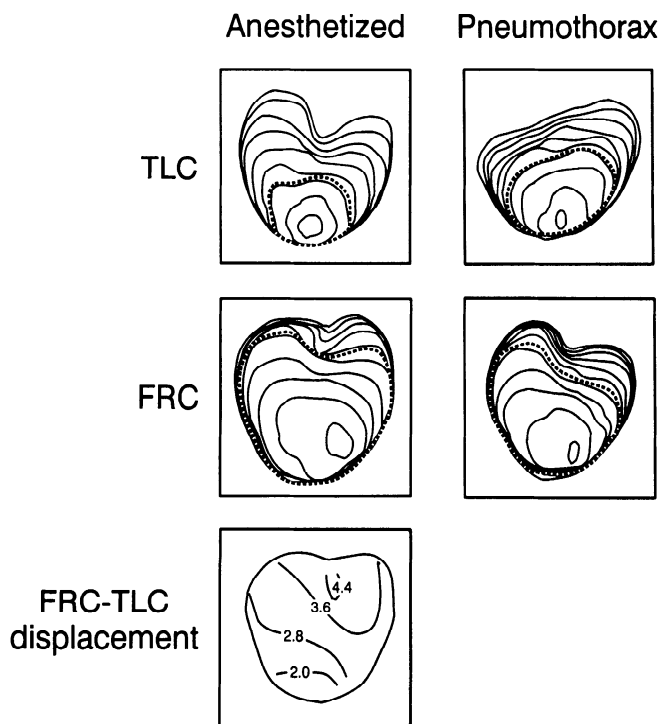


FIG. 3. Contour diagrams of diaphragm surface in prone dog at TLC and FRC in anesthetized and isovolume pneumothorax conditions. Level lines, outline of diaphragm in a series of 1.6-mm-thick transverse planes with an 8-mm separation. Dashed line, level of a reference location on the spine that remains stationary with changes in lung volume and body position. Cephalad displacement of diaphragm during a passive deflation from TLC to FRC in anesthetized dog is shown by level lines of displacement.

(Fig. 2). The volume of the mediastinum increases an average of 35 ml (14% of its TLC volume) in the supine dog and 60 ml (20% of its TLC volume) in the prone dog (Table 2) between TLC and FRC. In all dogs, in both the prone and supine postures, the increase in mediastinum volume occurs mostly in the heart or the "bulge" of the transverse area distribution of the mediastinum (Fig. 2). The caudal portion of the heart does not change axial position, but its cross-sectional area increases along most of its length and it extends farther toward the apex of the thorax. We have no explanation for the variability in mediastinum volume change across dogs.

Like a topographical plot of the surface of the earth, a contour plot of the diaphragm is a convenient means for displaying the details of the shape and elevation of the diaphragm. Contour plots like those shown in Figs. 3 and

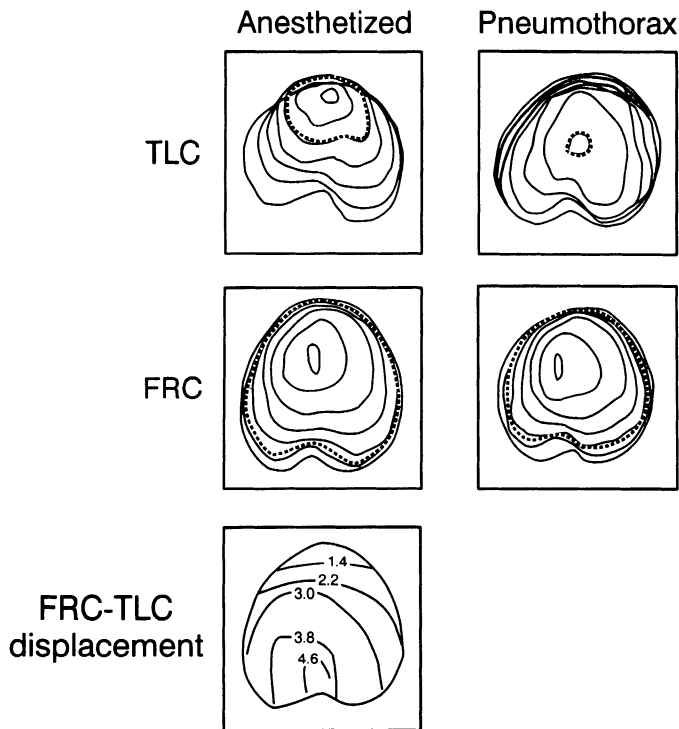


FIG. 4. Contour diagrams of diaphragm surface in supine dog at TLC and FRC in anesthetized and isovolume pneumothorax conditions. See Fig. 3 for further explanation.

4 were made by tracing the outline of the diaphragm surface in 1.6-mm-thick horizontal slices, beginning at the dome of the diaphragm and moving caudally by 8-mm increments. The contour lines appear close together where the diaphragm has a steep descent and widely spaced where the diaphragm is flatter. The dashed lines identify the level of a fixed position on the spine. This level does not change with lung volume or body position and is used as a reference elevation against which displacements of the diaphragm dome are evaluated. The caudal displacement of the diaphragm as it descends between FRC and TLC was calculated by superimposing the FRC and TLC contour plots and with use of the dome-to-reference elevation and is presented in Figs. 3 and 4 for the prone and supine anesthetized dog.

Because our isovolume pneumothorax protocol required that the animals be dead, we wanted to separate any postmortem chest wall changes from those due to the induction of pneumothorax. To do so we scanned the dogs at TLC and FRC after administering a lethal injection of barbiturate, but before we induced the pneumothorax. There was no difference in the rib cage, mediastinum, and diaphragm cross-sectional area distributions between the anesthetized and dead states. We conclude that postmortem alterations in the chest wall musculature had no effect on the general shape of the chest wall.

## DISCUSSION

The chest wall is the container of the lung that is formed by the rib cage, mediastinum, and diaphragm surfaces. We will discuss the effects of lung volume and posture on each component and the effect of abolishing the interaction between the lung and the chest wall by

isovolume pneumothorax. Finally, we will propose how the lung might distort to conform to the changes in the shape of the chest wall between TLC and FRC in the prone and supine anesthetized dog. A more detailed analysis of the deformation of the lung within the chest wall is presented in the companion paper by Liu et al. (11).

*Rib cage.* The rib cage is a stiff chest wall component and its shape at TLC and FRC, as judged by the transverse area distribution, is relatively unaffected by body posture and isovolume pneumothorax. At both lung volumes the shape of the rib cage of the prone and supine anesthetized dog are quite similar in the cephalad region. The caudal region of the prone rib cage is slightly smaller than the supine, possibly because of compression of the lower rib cage by the sling in the prone position. The rib cage changed little at TLC and FRC after pneumothorax (cross-sectional area increased an average of 5% in all dogs).

The transverse area of the rib cage increases monotonically with  $z$ , the axial distance from the apex of the thorax. The rib cage cross-sectional area distributions at TLC and FRC for the supine anesthetized dog are displayed together in Fig. 5. The ratio between FRC and TLC cross-sectional areas at a particular cephalocaudal location [ $\hat{A}_{\text{FRC}}(z)$  and  $\hat{A}_{\text{TLC}}(z)$ , respectively] remains nearly constant from the apex to the base of the thorax (average coefficient of variation across all dogs, 6%), and the rib cage deformation from TLC to FRC can be modeled as a uniform reduction in the rib cage cross-sectional area. This relationship between  $\hat{A}_{\text{FRC}}(z)$  and

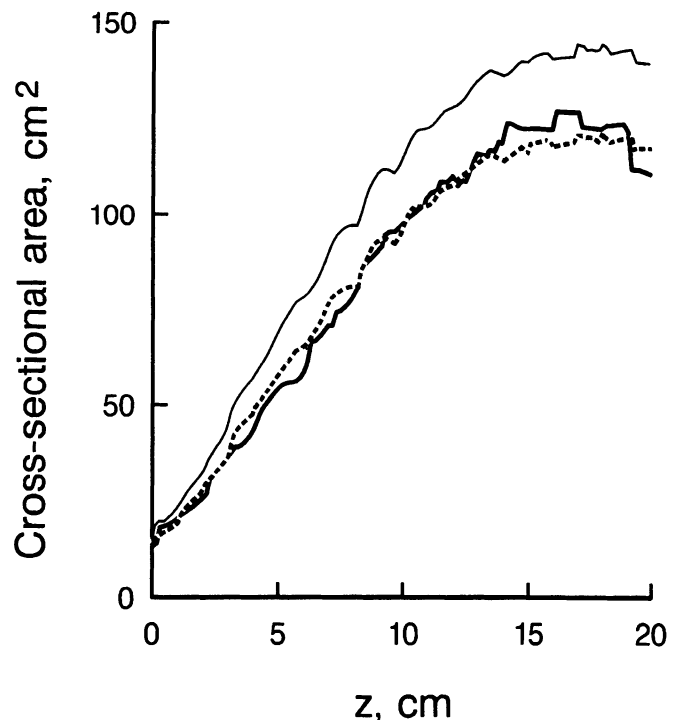


FIG. 5. Cross-sectional area of rib cage as a function of distance from apex of thorax at TLC (thin line) and FRC (thick line). Dashed line, area distribution that would result from a uniform proportional change in transverse area along length of rib cage between TLC and FRC. Volume bounded by rib cage, or area under cross-sectional area distribution, is equal for the model (dashed line) and the data at FRC.

$\tilde{A}_{TLC}(z)$  is described by the equation

$$\tilde{A}(z) = K_{RC} \tilde{A}_{TLC}(z) \quad (1)$$

where  $\tilde{A}(z)$  is the FRC cross-sectional area predicted by the model and  $K_{RC}$  is a constant. The FRC cross-sectional area distribution predicted by the rib cage model for the supine anesthetized dog ( $K_{RC} = 0.84$  for dog 4) is displayed with the measured TLC and FRC distributions in Fig. 5. The model for the rib cage described by Eq. 1 fits the FRC data from all the dogs in each body position quite closely. For the predicted rib cage volume to equal the actual volume at FRC ( $\tilde{V}_{FRC}$ ),  $K_{RC}$  must be defined by the relationship  $K_{RC} = \tilde{V}_{FRC}/\tilde{V}_{TLC}$ . The rib cage model parameter  $K_{RC}$  for the prone and supine anesthetized dog is presented in Table 3. Thus, despite the complex shape and motion of individual ribs (12), the shape changes of the rib cage as a whole during a passive deflation can be described simply as a uniform proportional change in rib cage cross-sectional area.

**Mediastinum.** During passive deflation of the lungs from TLC to FRC, mean pleural pressure decreases, and this decrease in pressure around the heart and great vessels causes blood flow to the mediastinum from other parts of the body. The values shown in Table 2 for large volume mechanical inflation are consistent with the relationship between intrathoracic blood volume and esophageal pressure changes reported by Warner et al. (15) for supine anesthetized dogs breathing spontaneously and during tidal volume mechanical ventilation.

Figure 6 presents photographs of a 1.6-mm-thick transverse section through the heart at a fixed level on the spine ( $z = 6.8$  cm) and documents the changes in the ventral-dorsal position of the heart in the prone and supine anesthetized dog at both lung volumes and with isovolume pneumothorax. The air-filled lung appears dark, the mediastinum and chest wall are light, and the trachea and bronchi appear as dark circles or ovals in the mediastinum near the spine. At FRC in the anesthetized dog, the cross-sectional area of the heart is larger but does not move a great deal within the transverse plane from its location at TLC. The cephalad motion of the lungs from TLC to FRC is identified in Fig. 6 by bronchi at FRC occupying what had been the trachea's position at TLC at the same vertebral level. The induction of isovolume pneumothorax collapses the lungs and creates a uniform pressure within the thorax and surrounding the heart without altering thoracic cavity volume. In the supine dog with pneumothorax the heart falls downward onto the collapsed lung, but there is little shift in the heart's position in the prone dog. This evidence supports the conclusions of Liu et al. (11) that

in the prone dog the heart is supported mostly by the sternum, and that in the supine dog part of the weight of the heart is borne by the lung tissue below the heart.

**Diaphragm.** Diaphragmatic shape changes between TLC and FRC lung volumes are more difficult to quantify conveniently than rib cage changes. In each body position in the anesthetized condition, we visually compared the contour plots of the diaphragm at TLC with those at FRC (Figs. 3 and 4), noting the shape and  $z$  (cephalocaudal) displacement of the diaphragm, as well as the position and displacement of the dome of the diaphragm. The central region of the diaphragm was flatter at FRC than at TLC in all dogs. A flatter diaphragm is defined as having more cross-sectional area contained by the first few isobars below the dome of the diaphragm and isobars that are more widely spaced than a more curved or tapered diaphragm. Because the origin of the diaphragm is oriented in the thorax such that the ventral portion is cephalad of the dorsal portion, this shape change is accomplished by the dorsal region displacing more than the ventral portion between TLC and FRC, regardless of body position (Figs. 3 and 4).

The regional cephalocaudal diaphragm displacement is shown in the lower left panel in Figs. 3 and 4. These diagrams were constructed by superimposing the FRC and TLC contours and using the dome elevation above the reference level to calculate displacement. The dome of the diaphragm displaced cranially an average of 2.1 cm at FRC relative to its TLC position in both body positions (with a range of 1.6–2.6 cm supine and 1.8–2.4 cm prone). In addition, the dome shifted dorsally from near the ventral surface of the rib cage at TLC to a more central location at FRC in all dogs, with the exception of dog 3 while prone, where the dome did not shift in the dorsal/ventral direction between TLC and FRC.

Hubmayr and co-workers determined diaphragm motion in the prone and supine anesthetized dog during mechanical ventilation (5) and during a passive deflation from TLC to FRC (6) from lateral projection fluoroscopic images. In both body positions during mechanical ventilation the dorsal diaphragm region had a larger excursion than the ventral regions. During passive lung deflation from TLC in the supine dog, the dorsal portion of the diaphragm also had a larger displacement than the ventral region, and they noted a change in the shape of the diaphragm at FRC from that at TLC. They did not find large diaphragmatic shape changes in the prone dog. In contrast to these findings in the dog, Froese and Bryan (8) found that, in supine anesthetized and paralyzed humans, the displacement of the silhouette of the passive diaphragm between FRC and end tidal volume was greatest in the ventral region, and the motion became uniform for large volume ventilation.

At each of the lung volumes in the anesthetized dog, the diaphragm was less flat prone than supine, indicated by visually noting a more gradual increase in cross-sectional area in the prone posture (Fig. 2) and by the contour diagrams (Figs. 3 and 4). The decreased contour line spacing and increased number of contour lines below the reference level in the prone anesthetized dog indicate that the diaphragm is steeper in the dorsal region and

TABLE 3.  $K_{RC}$  for anesthetized dog

Dog No.	Supine	Prone
1	0.86	0.81
2	0.90	0.84
3	0.82	0.82
4	0.84	0.83
5	0.85	0.84
6	0.84	0.78
Means $\pm$ SD	0.85 $\pm$ 0.03	0.82 $\pm$ 0.02

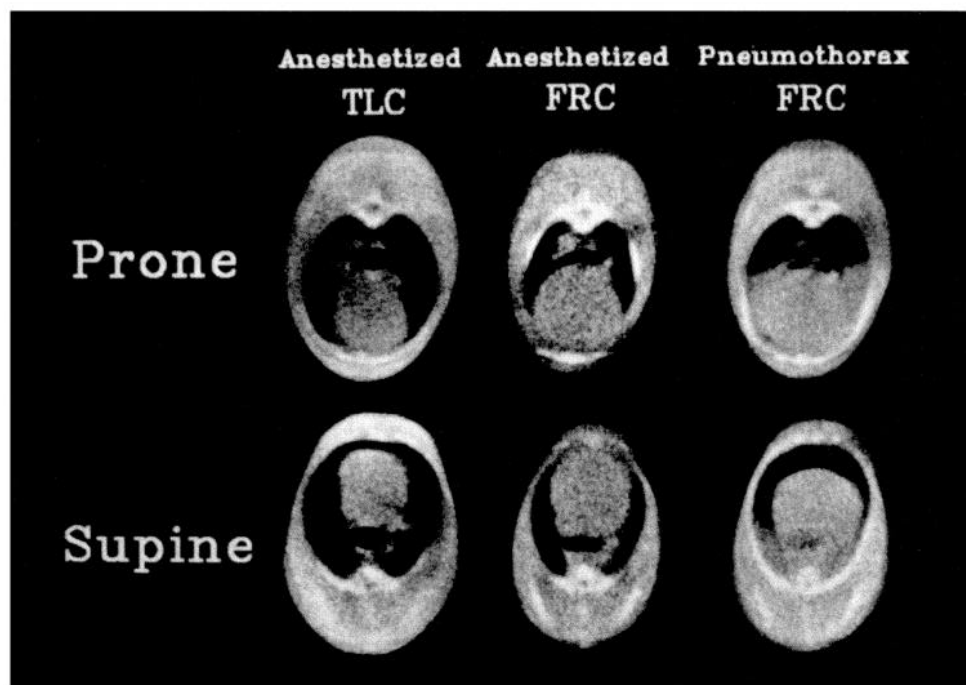


FIG. 6. Photographs of 1.6-mm-thick transverse planes through DSR images of prone and supine dog at a constant vertebral level. Air-filled lung or thorax appears dark, rib cage and mediastinum are gray, and bony structures are white. Any dorsal/ventral and lateral motion of the mediastinum accompanying lung volume or postural changes or after pneumothorax is shown.

extends farther in the cephalocaudal direction at both lung volumes than in the supine dog, presumably because the dorsal zone of apposition is smaller in the prone dog. In three of the dogs at FRC and one at TLC, the dome is located more ventrally in the prone posture than the supine posture. The axial position of the dome of the diaphragm in the prone and supine body positions is approximately the same in *dog 4* (Figs. 3 and 4), but the range for all the dogs was 0–11 mm more cephalad position in the prone position at FRC (mean 4.5 mm) and 1.6–6.4 mm at TLC (mean 4.2 mm). In summary, the diaphragm is less flat in the prone posture at both FRC and TLC relative to the supine posture due to a cephalad shift in the ventral diaphragm and a caudad shift in the dorsal diaphragm.

The diaphragm is a membranous structure that offers little resistance to bending, and thus its shape is governed by its surroundings. The shape of the diaphragm is influenced by the shape and deformability of the lungs and abdomen, the tension in the diaphragm, and the distribution of transdiaphragmatic pressure over the diaphragm's surface. At TLC the lung is quite stiff (10), the passive diaphragm is under little tension, and mean transdiaphragmatic pressure is small. The diaphragm conforms to the lung's shape as if it were a sheet draped over the caudal lung surface and held in place by the abdominal contents. The lung is stiff, so changes in lung shape have a strong influence on diaphragm shape. Because the dome of the diaphragm is convex toward the head, transdiaphragmatic pressure ( $P_{di} = P_{ab} - P_{pl}$ , where  $P_{ab}$  is abdominal pressure and  $P_{pl}$  is pleural pressure) cannot be negative. The vertical gradient in  $P_{di}$  is simply the difference between the  $P_{ab}$  and  $P_{pl}$  gradients

$$\frac{\partial P_{di}}{\partial h} = \frac{\partial P_{ab}}{\partial h} - \frac{\partial P_{pl}}{\partial h} \quad (2)$$

where  $h$  is vertical height.

If we assume that the average  $P_{di}$  at TLC is essentially zero and accept that  $P_{di}$  cannot be negative because of the diaphragm's shape, then there can be no vertical gradient in  $P_{di}$  at TLC. Therefore, the vertical gradient in  $P_{ab}$  (assumed to be 1 cmH<sub>2</sub>O/cm) must be balanced by an equal gradient in  $P_{pl}$ . When the dog is rotated from supine to prone, the shape of the lung is altered in response to a reversal in the direction of these gradients.

In intact anesthetized dogs, Chevalier et al. (1) reported that individual lobes of the lung were uniformly expanded at TLC in both the prone and supine body postures, but that the overall lung shape changed with posture, presumably as a result of the lobes shifting and rotating relative to each other. They observed the silhouette of the diaphragm in lateral X-ray images when the dogs were rotated from supine to prone and noted a leverlike diaphragm motion where ventral regions moved cephalad and dorsal regions moved caudad like the shift between Figs. 4 and 3.

At FRC the lung is more deformable but is no longer the only factor determining the diaphragm's shape. Tension in the passive diaphragm is larger and  $P_{di}$  is higher than at TLC, so the diaphragm responds less to changes in the  $P_{di}$  distribution. At FRC the hydrostatic gradient in  $P_{ab}$  is balanced partly by a gradient in  $P_{pl}$  and partly by a gradient in  $P_{di}$  (Eq. 2). As at TLC, these gradients are reversed when the dog is rotated from supine to prone. The diaphragm shape changes after rotation are similar at FRC and TLC in all dogs. Hoffman and Ritman (3) superimposed 1.5-mm-thick midsagittal plane DSR images of an anesthetized dog at FRC lying prone and supine and observed that the dog's diaphragm shifted like a lever arm fixed about the central head-foot axis, such that the ventral regions of the diaphragm were more cephalad and dorsal regions more caudad in the prone posture.

Bilateral pneumothorax removes the coupling between the lung and the chest wall and creates a uniform Ppl distribution. We produced isovolume pneumothorax in five dogs lying supine but rotated only one of these dogs prone. The shape of the diaphragm is relatively unaffected by pneumothorax at the FRC respiratory system volume (Figs. 3 and 4). The most dramatic changes in the diaphragm occur with pneumothorax at TLC. At TLC in the supine dogs the dome of the diaphragm, which is ventral and in a nondependent region, displaces dorsally toward the center of the thorax and caudad  $\sim 1.6$  cm<sup>1</sup> with pneumothorax. The central region of the diaphragm is flatter after pneumothorax than in the supine anesthetized condition and evenly tapered on all sides. The slight right lateral shift of the dome of the diaphragm seen at prone FRC in *dog 4* (Fig. 3) was detected in only one other dog. In contrast to the supine posture, pneumothorax in the prone posture at TLC displaced the dome of the diaphragm toward the ventral rib cage surface and 2.56 cm cephalad, and the shape of the diaphragm became more steeply sloped on the lateral and dorsal extremes.

Just as with a rotation from the prone to supine posture, the diaphragm changes shape with pneumothorax in response to changes in the factors influencing its shape: the lung, abdomen, diaphragmatic tension, and Pdi. In the prone dog the weight of the abdomen rests on the sternum and abdominal wall, and the lung has little if any role in its support. In the supine dog the weight of the abdomen is borne by the diaphragm, rib cage, and lung. Pneumothorax removes the support to the diaphragm and abdomen offered by the lung.

The magnitude and distribution of the Pdi also affect the shape of the diaphragm. Because any air escaping from the lungs enters the pleural space, thoracic cavity volume remains constant as we induce isovolume pneumothorax. Thus, because the total volume of the thorax and abdomen remains unchanged, the average Ppl, Pab, and Pdi are not altered by the pneumothorax, but the distribution of pressure over the diaphragm and rib cage surfaces changes. The last term on the right in *Eq. 2* is reduced to zero with pneumothorax, and the vertical gradient in Pdi increases. The increased vertical gradient of Pdi with pneumothorax produces a decrease in Pdi in the nondependent region of the diaphragm and an increase in Pdi in the dependent region. If a vertical gradient in Ppl were present in the intact anesthetized dog and then abolished with pneumothorax, the diaphragm would respond to these pressure changes by displacing caudad in the nondependent regions and cephalad in the dependent regions.

The diaphragmatic shape changes with pneumothorax at the TLC volume indicate that pneumothorax removed the support provided by the lung, abolished a Ppl gradient present in the anesthetized dog, and altered the vertical gradient in Pdi as described by *Eq. 2*. In the

supine dog the dome of the diaphragm displaces caudad with pneumothorax in response to a decrease in Pdi in the nondependent region of the diaphragm, and the dorsal diaphragm displaces headward due to an increase in Pdi in this dependent region, flattening the diaphragm. After pneumothorax the dome is more centrally located in the thorax due to the cephalocaudal shifts of the diaphragm caused by changes in the Pdi distribution. In the prone position, the dome of the diaphragm, now located in the dependent region, displaces cephalad while the nondependent regions of the diaphragm near the spine displace caudad.

To our knowledge no one has tried to measure a vertical gradient in Ppl at TLC in the recumbent dog. However, Hyatt and co-workers (7) measured a vertical gradient in Pes in head-up dogs at TLC. Evidence that Ppl is not uniform in the supine dog is given by Fig. 6, which shows that the heart is in the midthorax in TLC and FRC and that it drops down after pneumothorax when pleural pressure is uniform. Hoffman (2) found little or no evidence of an associated vertical gradient in the volume distribution in the lung at TLC in prone and supine dogs. Most probably, the lung is so stiff at TLC that it is uniformly expanded, despite a nonuniform Ppl distribution.

The diaphragm shape changes at FRC after isovolume pneumothorax are more subtle than those at TLC. The ventral portion of the diaphragm moves caudad slightly and the diaphragm just dorsal to the dome moves cephalad, giving the appearance that the diaphragm slumps gently toward the spine when the Ppl gradient and interaction with the lung are removed. In all but one of the dogs at FRC in the supine position, the position of the dome of the anesthetized diaphragm is nearly identical before and after isovolume pneumothorax (Figs. 3 and 4). In *dog 2*, the exception, the diaphragm dome displaced caudad 1 cm with supine pneumothorax, due to a 200-ml air leak into the respiratory system volume with the induction of pneumothorax, but the shape changes were similar to the other dogs. In the one prone dog with pneumothorax, the shape and position of the diaphragm at FRC also changed only slightly from the anesthetized state.

There are three explanations for smaller differences between the anesthetized and pneumothorax conditions at FRC than at TLC. First, if the vertical gradient of Ppl were smaller at FRC than TLC in the anesthetized dog, pneumothorax would cause a smaller change in the distribution of Pdi over the diaphragm surface. Wiener-Kronish et al. (16) measured Ppl gradients of 0.46 and 0.23 cmH<sub>2</sub>O/cm in supine and prone anesthetized dogs at FRC, respectively. The gradient in Ppl at TLC has not been measured but may be 1 cmH<sub>2</sub>O/cm as discussed earlier. Second, the magnitude of the change in the Pdi gradient with pneumothorax may be smaller compared with the mean Pdi at FRC than at TLC. In a passive deflation of the lungs or thorax from TLC to FRC, mean Pdi increases as the diaphragm moves cephalad. At small Pdi (i.e., at TLC), a change in the gradient of Pdi produces significant shape changes. When the Pdi is large compared with the variation of pressure on the

<sup>1</sup> Dog 2 had a 200-ml air leak into the respiratory system volume with the induction of pneumothorax. Together, the pneumothorax and increase in thoracic volume produced a 3.1-cm displacement of the dome of the diaphragm. Although the magnitude of diaphragm displacement was affected by the air leak, the shape changes after pneumothorax were identical to those in the other dogs.

TABLE 4.  $V_{FRC}/V_{TLC}$  and  $K_L$  for anesthetized dog

Dog No.	Supine		Prone	
	$V_{FRC}/V_{TLC}$	$K_L$	$V_{FRC}/V_{TLC}$	$K_L$
1	0.49	0.79	0.44	0.76
2	0.39	0.73	0.37	0.72
3	0.46	0.77	0.42	0.75
4	0.39	0.73	0.29	0.66
5	0.37	0.72	0.37	0.72
6	0.42	0.75	0.36	0.71
Means $\pm$ SD	0.42 $\pm$ 0.05	0.75 $\pm$ 0.03	0.38 $\pm$ 0.05	0.72 $\pm$ 0.04

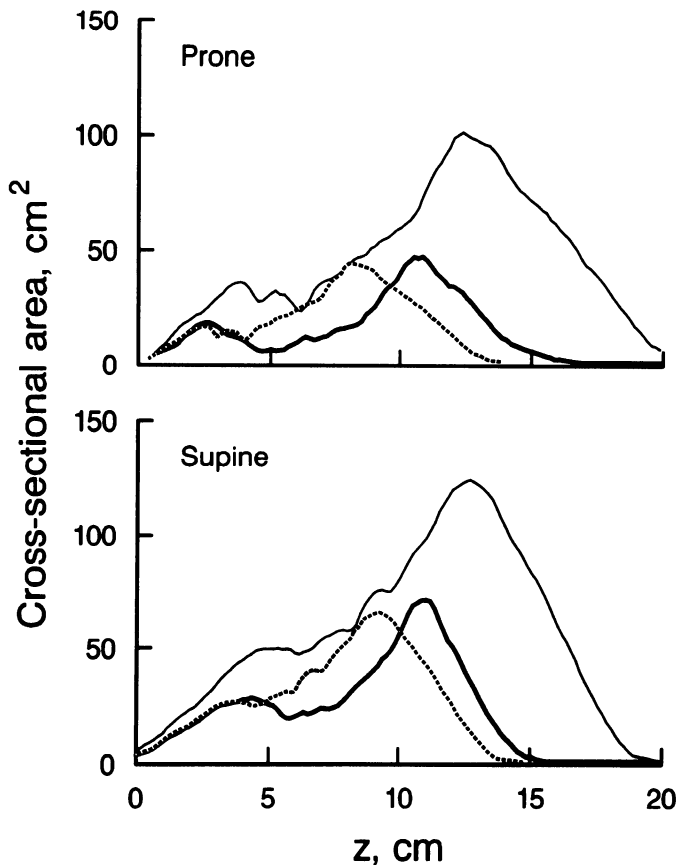


FIG. 7. Cross-sectional area of the lung as a function of distance from apex of thorax at TLC (thin line) and FRC (thick line) and for a lung that has the same volume as that observed at FRC but shape of lung at TLC (dashed line).

diaphragm surface, the shape of the diaphragm is less sensitive to changes in the gradient. Finally, we have assumed that the pleural pressure is uniform over the diaphragm surface after pneumothorax at both TLC and FRC thoracic cavity volumes. There is little interaction between the collapsed lung and the diaphragm at TLC, but as the diaphragm moves cephalad to FRC, it may touch and be influenced by the collapsed lung and mediastinum, especially in the dorsal region.

**Summary and implications for lung deformation.** The rib cage, mediastinum, and diaphragm each deform in a unique way during a passive deflation of the lungs from TLC to FRC in the prone or supine anesthetized dog. The rib cage response can be modeled as a uniform fractional reduction in transverse area from apex to base, whereas the general shape remains unchanged. In the

upper and lower thorax the mediastinum is small and remains unchanged with lung volume. In the midthorax, the mediastinum occupies a large portion of the thoracic cavity and increases in volume as lung volume decreases. The diaphragm surface displaces cephalad nonuniformly, more in the dorsal portion than the ventral, which causes a flattening of its shape at FRC relative to that at TLC. How would this complex shape change in the lung's container cause the lung to distort?

As a first approximation, we considered the lung to be a homogeneous elastic material which fills the chest wall and deforms from TLC to FRC in an isotropic manner. If the lung at TLC were a stack of transverse slices from apex to base, each slice with a cross-sectional area  $A_{TLC}(z)$  and a thickness  $L_{TLC}(z)$ , an isotropic deformation would reduce each lung slice by an equal fraction in all directions. With the location of the apex fixed and no deformation gradients allowed, the new transverse area and thickness of a slice at a cephalocaudal position  $z$  is given by

$$A(z) = K_L^2 A_{TLC}(z) \quad (3)$$

$$L(z) = K_L L_{TLC}(z) \quad (4)$$

where  $K_L$  is the constant of proportionality for the lung.  $K_L$  is defined by the restriction that the volume ( $V$ ) of the isotropically reduced lung equals the true lung volume at FRC

$$K_L = \left[ \frac{V_{FRC}}{V_{TLC}} \right]^{1/3} \quad (5)$$

Values for  $V_{FRC}/V_{TLC}$  and  $K_L$  are reported in Table 4 for the prone and supine anesthetized dogs.

The transverse area of the lung at TLC and FRC is shown in Fig. 7 against axial distance from the lung apex for dog 4 in the prone and supine positions. The dashed line is the isotropically reduced lung. According to Eqs. 3-5, the lung volume, or area under the curve in Fig. 7, is identical for the model and the FRC data. If the chest wall components changed uniformly and by the same fraction between TLC and FRC, this might be a plausible model for the deflation of the lung. But, as one can see in the figure, an isotropic reduction of the TLC lung does not fit the shape of the chest wall at FRC. An isotropic reduction shrinks the length of the lung more than necessary and does not squeeze it enough in the region around the heart where mediastinum volume increases. In another article, Liu et al. (11) present an analysis of the deformation required to fit the lung to the shape of the chest wall at FRC.

The authors thank Dr. Eric Hoffman for reconstructing the DSR images, Peter Bergsland and Daniel Olson for help in image analysis, and Dr. Theodore Wilson for discussions about the data and contributions to the manuscript.

This study was supported by National Heart, Lung, and Blood Institute Grants HL-04664 and HL-07222.

Address for reprint requests: S. S. Margulies, Mayo Clinic, Rochester, MN 55905.

Received 17 January 1989; accepted in final form 21 December 1989.

## REFERENCES

1. CHEVALIER, P. A., J. R. RODARTE, AND L. D. HARRIS. Regional lung expansion at total lung capacity in intact vs. excised canine lungs. *J. Appl. Physiol.* 45: 363-369, 1978.
2. HOFFMAN, E. A. Effect of body orientation on regional lung expansion: a computed tomographic approach. *J. Appl. Physiol.* 59: 468-480, 1985.
3. HOFFMAN, E. A., AND E. L. RITMAN. Effect of body orientation on regional lung expansion in dog and sloth. *J. Appl. Physiol.* 59: 481-491, 1985.
4. HOFFMAN, E. A., L. J. SINAK, R. A. ROBB, AND E. L. RITMAN. Noninvasive quantitative imaging of shape and volume of lungs. *J. Appl. Physiol.* 54: 1414-1421, 1983.
5. HUBMAYR, R. D., J. R. RODARTE, B. J. WALTERS, AND F. M. TONELLI. Regional ventilation during spontaneous breathing and mechanical ventilation in dogs. *J. Appl. Physiol.* 63: 2467-2475, 1987.
6. HUBMAYR, R. D., B. J. WALTERS, P. A. CHEVALIER, J. R. RODARTE, AND L. E. OLSON. Topographical distribution of regional lung volume in anesthetized dogs. *J. Appl. Physiol.* 54: 1048-1056, 1983.
7. HYATT, R. E., E. BAR-YISHAY, AND M. D. ABEL. Influence of the heart on the vertical gradient of transpulmonary pressure in dogs. *J. Appl. Physiol.* 58: 52-57, 1985.
8. FROESE, A. B., AND A. C. BRYAN. Effects of anesthesia and paralysis on diaphragmatic mechanics in man. *Anesthesiology* 41: 242-255, 1974.
9. KRAYER, S., K. REHDER, K. C. BECK, P. D. CAMERON, E. P. DIDIER, AND E. A. HOFFMAN. Quantification of thoracic volumes by three-dimensional imaging. *J. Appl. Physiol.* 62: 591-598, 1987.
10. LAI-FOOK, S. J., T. A. WILSON, R. E. HYATT, AND J. R. RODARTE. Elastic constants of inflated lobes of dog lungs. *J. Appl. Physiol.* 40: 508-513, 1976.
11. LIU, S., S. S. MARGULIES, AND T. A. WILSON. Deformation of the dog lung in the chest wall. *J. Appl. Physiol.* 68: 1979-1987, 1990.
12. MARGULIES, S. S., J. R. RODARTE, AND E. A. HOFFMAN. Geometry and kinematics of dog ribs. *J. Appl. Physiol.* 67: 707-712, 1989.
13. MEAD, J. Mechanical properties of lungs. *Physiol. Rev.* 41: 281-330, 1961.
14. RODARTE, J. R., R. D. HUBMAYR, D. STAMENOVIC, AND B. WALTERS. Regional lung strain in dogs during deflation from total lung capacity. *J. Appl. Physiol.* 58: 164-172, 1985.
15. WARNER, D. O., S. KRAYER, K. REHDER, AND E. L. RITMAN. Chest wall motion during spontaneous breathing and mechanical ventilation in dogs. *J. Appl. Physiol.* 66: 1179-1189, 1989.
16. WIENER-KRONISH, J. P., M. A. GROPPER, AND S. J. LAI-FOOK. Pleural liquid pressure in dogs measured using a rib capsule. *J. Appl. Physiol.* 59: 597-602, 1985.

